

# Experiments on floating bed rotating drums using magnetic particle tracking

**Citation for published version (APA):**

Nijssen, T. M. J., van Dijk, M. A. H., Kuipers, H. A. M., van der Stel, J., Adema, A. T., & Buist, K. A. (2022). Experiments on floating bed rotating drums using magnetic particle tracking. *AIChE Journal*, 68(5), Article e17627. <https://doi.org/10.1002/aic.17627>

**Document license:**  
CC BY

**DOI:**  
[10.1002/aic.17627](https://doi.org/10.1002/aic.17627)

**Document status and date:**  
Published: 01/05/2022

**Document Version:**  
Publisher's PDF, also known as Version of Record (includes final page, issue and volume numbers)

**Please check the document version of this publication:**

- A submitted manuscript is the version of the article upon submission and before peer-review. There can be important differences between the submitted version and the official published version of record. People interested in the research are advised to contact the author for the final version of the publication, or visit the DOI to the publisher's website.
- The final author version and the galley proof are versions of the publication after peer review.
- The final published version features the final layout of the paper including the volume, issue and page numbers.

[Link to publication](#)

**General rights**

Copyright and moral rights for the publications made accessible in the public portal are retained by the authors and/or other copyright owners and it is a condition of accessing publications that users recognise and abide by the legal requirements associated with these rights.

- Users may download and print one copy of any publication from the public portal for the purpose of private study or research.
- You may not further distribute the material or use it for any profit-making activity or commercial gain
- You may freely distribute the URL identifying the publication in the public portal.

If the publication is distributed under the terms of Article 25fa of the Dutch Copyright Act, indicated by the "Taverne" license above, please follow below link for the End User Agreement:

[www.tue.nl/taverne](http://www.tue.nl/taverne)

**Take down policy**

If you believe that this document breaches copyright please contact us at:



[openaccess@tue.nl](mailto:openaccess@tue.nl)

providing details and we will investigate your claim.

## RESEARCH ARTICLE

## Particle Technology and Fluidization

## Experiments on floating bed rotating drums using magnetic particle tracking

Tim M. J. Nijssen<sup>1</sup>  | Mark A. H. van Dijk<sup>1</sup> | Hans A. M. Kuipers<sup>1</sup> |  
Jan van der Stel<sup>2</sup> | Allert T. Adema<sup>2</sup> | Kay A. Buist<sup>1</sup> 

<sup>1</sup>Multiphase Reactors Group, Department of Chemical Engineering & Chemistry, Eindhoven University of Technology, Eindhoven, The Netherlands

<sup>2</sup>Research and Development, Tata Steel Europe, IJmuiden, The Netherlands

## Correspondence

Kay A. Buist, Multiphase Reactors Group, Department of Chemical Engineering & Chemistry, Eindhoven University of Technology, PO Box 513, 5600 MB Eindhoven, The Netherlands.  
Email: k.a.buist@tue.nl

## Funding information

Tata Steel, Grant/Award Number: S16046

## Abstract

Magnetic particle tracking (MPT) was employed to study a rotating drum filled with cork particles, using both air and water as interstitial medium. This noninvasive monitoring technique allows for the tracking of both particle translation and rotation in dry granular and liquid–solid systems. Measurements on the dry and floating bed rotating drum were compared and detailed analysis of the bed shape and velocity profiles was performed. It was found that the change of particle–wall and particle–particle interaction caused by the presence of water significantly affects the bed behavior. The decreased friction leads to slipping of the particles with respect to the wall, rendering the circulation rate largely insensitive to increased drum speed. It was also found that the liquid–particle interaction is determining for the behavior of the flowing layer. The well-defined experiments and in-depth characterization performed in this study provide an excellent validation case for multiphase flow models.

## KEYWORDS

floating particle bed, liquid–solid systems, magnetic particle tracking, particle dynamics, rotating drum

## 1 | INTRODUCTION

The applications of rotating drums for handling and processing of granular materials are numerous. These devices, consisting of a cylinder rotating about its axis, are employed for mixing, coating, drying, calcination, grinding, granulation, and many other industrial processes. The behavior of dry granular matter in a rotary drum is well described in literature. Many studies, both experimental<sup>1,2</sup> and numerical<sup>3–5</sup> in nature, have been dedicated to the granular flow inside the drum. Based on the rotational velocity, filling degree and properties of the granules different particle flow patterns are prevailing, ranging from a slipping bed at low velocity to centrifuging behavior at the highest rotational speed. The intermediate rolling regime is often of special interest, due to its fast mixing and favorable energy consumption.<sup>3</sup> In

this regime, the bed is divided in a densely-packed layer at the drum wall and a freely rolling active layer at the bed surface. More complex flow behavior is observed in studies involving nonspherical particles<sup>6</sup> or cohesive materials.<sup>7</sup> In addition to characterization of the flow patterns, many studies have been dedicated to the mixing, mass and heat transfer behavior in these devices.<sup>5,8,9</sup>

The possible applications of rotating drum devices are not limited to gas–solid systems. Liquid–solid rotating drums, most prevalent using water as the interstitial medium, have been presented as a promising contactor/reactor design for several biochemical processes, including cultivation of plant cells,<sup>10</sup> treatment of contaminated soil,<sup>11</sup> and bioleaching of various metal ores.<sup>12–14</sup> Generally, such units utilize a sparging mechanism for introducing oxygen into the vessel. The liquid–solid rotating drum has been selected as a suitable device for

This is an open access article under the terms of the Creative Commons Attribution License, which permits use, distribution and reproduction in any medium, provided the original work is properly cited.

© 2022 The Authors. *AIChE Journal* published by Wiley Periodicals LLC on behalf of American Institute of Chemical Engineers.

these processes due to its gentle agitation yet effective mass transfer rates.<sup>10</sup>

Finally, rotating drum devices are often employed in geologic research to study flowing layers or avalanches of soil and debris.<sup>15–17</sup> Also in this application, the influence of the interstitial medium on the granular flow is of major interest, contributing to the study of a wide variety of naturally occurring phenomena, such as submarine landslides.

While research on rotating gas–solid rotating drums is extensive, much less is known about rotating drum flow with liquid interstitial media. Breu et al.<sup>18,19</sup> studied the formation, growth and decay of patterns in rotating slurries of monodisperse glass beads. They found different ring-like patterns formed in the drum, depending on the rotation speed and liquid viscosity. However, no underlying mechanics could be identified. Jain et al.<sup>20</sup> found similar results for bidisperse mixtures of particles. The authors also found that size-based segregation is faster in liquids than in air and provide an analysis of the segregation and diffusion velocities to explain this finding. In addition, Finger and Stannarius<sup>21</sup> found that while the influence of fluid viscosity on segregation behavior is significant, no influence is observed of the fluid density.

An in-depth analysis of avalanche behavior in liquid-filled drums was provided by Courrech du Pont et al.<sup>22</sup> In this study, avalanches were divided into three regimes based on the solid/liquid density ratio  $r = \sqrt{\rho_p/\rho_f}$  and the Stokes number (Equation 1). The latter signifies the ratio of particle inertia and fluid viscosity, based on the densities  $\rho$ , angle of repose  $\theta$ , particle diameter  $d_p$ , and fluid dynamic viscosity  $\mu_f$ .

$$St = \frac{\sqrt{\rho_p} \sqrt{\Delta\rho g \sin\theta} d_p^{3/2}}{18\sqrt{2}\mu_f} \quad (1)$$

In the free-falling regime (high Stokes number and density ratio), no influence of the interstitial liquid is observed, as is the case for dry granular matter. For liquid–solid drums (low density ratio), avalanches are either in the viscous limit regime (low Stokes number) or the inertial limit regime (high Stokes number). This study shows that influence of the interstitial medium can range from negligible to highly significant based on the particle and fluid properties. In a later study of Jain et al.,<sup>23</sup> focus was on the flowing granular layer rather than avalanches. This study was conducted using high-density steel beads, and the authors found little influence of the interstitial liquid on the flow dynamics, especially for larger particles (>2 mm).

The behavior of a dry rotating drum is often characterized by the Froude number (2). This dimensionless group signifies the ratio between particle inertia and gravity, based on the drum angular velocity  $\Omega$ , drum radius  $R$ , and gravitational acceleration  $g$ . As this group does not consider influences of the interstitial medium inertia and viscosity, its application in a liquid–solid system is precarious. Based on experimental and numerical results, Juarez et al.<sup>24</sup> developed an adjusted Froude number, including the effects of particle friction, as the sin of the angle of repose, drum volume fill fraction  $f$ , and the particle–fluid density difference  $\Delta\rho$  (Equation 3). They found that the transition toward the centrifuging regime was predicted reasonably well by this adjusted Froude number for both dry and immersed cases.

The expression in Equation (3) was modified slightly from the original to account for floating particles without producing negative values.

$$Fr = \frac{\Omega^2 R}{g} \quad (2)$$

$$Fr_{adj} = Fr \left( \frac{\sin\theta \sqrt{1-f}}{\Delta\rho/\rho_p} \right) \quad (3)$$

Liao and Chou<sup>25–28</sup> performed different experiments using particle tracking velocimetry (PTV) in a quasi-2D rotating drum. They studied the behavior of monodisperse glass beads in water and different water/glycerin mixtures in order to establish the influence of viscosity on the drum dynamics. Apart from observing the avalanche regimes described by Courrech du Pont et al.,<sup>22</sup> the authors also composed a regime map showing the transition to a uniform suspension regime.<sup>28</sup> It was found that the granular temperature decreases with fluid viscosity, yet particle mixing is promoted.<sup>25</sup> Furthermore, experiments using bidisperse particle mixtures have shown that size-based segregation is weaker in more viscous liquids, while density-based segregation grows stronger. Finally, Parsons et al.<sup>29</sup> studied the liquid–solid mass transfer in a partially filled drum with baffles using dissolution experiments. They found a linear relationship between the mass transfer coefficient and the rotation speed, but no influence of the slurry solids volume fraction.

In the aforementioned studies, experiments have been conducted using glass and steel beads in water and water/glycerin mixtures. In order to further explore the influence of the interstitial medium on bed dynamics, this study focuses on particles with a lower density than the fluid phase, that is, floating particle beds. Magnetic particle tracking (MPT) is used to obtain information on the particle movement in a rotating drum filled with water and cork spheres, as well as the dry cork spheres. MPT is a noninvasive monitoring technique which yields the time-resolved trajectory of a single magnetic marker.<sup>30</sup> Furthermore, MPT also gives information on the tracer orientation and rotation rate.<sup>31</sup> These experiments show the application of MPT in liquid–solid systems, as well as provide a basis for further study of dynamic immersed particle flow.

## 2 | METHODS

### 2.1 | Magnetic particle tracking

In MPT, the magnetic field generated by a single tracer particle is measured by an array of sensors. Using these data, the position and orientation of the tracer can then be reconstructed by treating the particle as a magnetic dipole. The detector used in this study has been described extensively by Buist et al.<sup>30</sup> It consists of a cylindrical array of 72 anisotropic magnetic resonance (AMR) sensors, positioned in four horizontal rings surrounding the drum. The inner radius and height of the array are 0.26 and 0.45 m, respectively. The magnetic field strength is measured at 1 kHz, which is consecutively down-sampled to 50 Hz.

The reconstruction of the tracer position and orientation from the magnetic field strength data is an iterative process, starting from an initial guess. The magnetic field strength corresponding to the assumed position and orientation is calculated and compared with the measured signal. Equation 4 gives the magnetic field  $H$  generated by a magnet with position  $\vec{r}_p$  and orientation  $\vec{e}_p$ , observed at sensor position  $\vec{r}_s$ . Here,  $\mu_m$  is the tracers magnetic moment (in  $A \cdot m^2$ ), and  $\vec{r}_{ps} = \vec{r}_p - \vec{r}_s$  is the vector between the sensor and the tracer. For further processing, the magnetic field is nondimensionalized using the magnetic moment and the sensor arrays typical size  $L$  (Equation 5). The theoretical sensor reading is obtained by taking the inner product of the field strength with the sensor orientation  $\vec{e}_s$ , as shown in Equation (6).

$$\vec{H}(\vec{e}_p, \vec{r}_{ps}) = \frac{\mu_m}{4\pi} \left( -\frac{\vec{e}_p}{|\vec{r}_{ps}|^3} + \frac{3(\vec{e}_p \cdot \vec{r}_{ps})\vec{r}_{ps}}{|\vec{r}_{ps}|^5} \right) \quad (4)$$

$$\vec{H}^* = \vec{H} \frac{4\pi L^3}{\mu_m} \quad (5)$$

$$S_{th}^*(\vec{e}_p, \vec{r}_{p,s}, \vec{e}_s) = \vec{H}^*(\vec{e}_p, \vec{r}_{ps}) \cdot \vec{e}_s \quad (6)$$

The true tracer position and orientation are obtained through minimization of the difference between theoretical and measured signals. The estimated position approaches the actual tracer position as  $S_{th}^*$  approaches the measured value  $S_m^*$  for every sensor. To assess the quality of the estimate, the chance of obtaining a better estimate than  $S_{th}^*$  is calculated using the standard deviation of the measurement  $\sigma_m^*$  (Equation 7). The terms  $\langle S \rangle$  denote the average over all sensors and are used to correct for any stray fields. The final quality function  $Q$  (Equation 8) is obtained by taking the root mean square (RMS) of  $P$  for every sensor. A small value for this parameter reflects an accurate reconstruction of the tracer position and orientation from the magnetic field strength data. A Sequential Quadratic Programming (SQP) in MATLAB<sup>®</sup> is used to minimize  $Q$ , that is, find the optimal estimate for position and orientation.

$$P = \text{erf} \left( \frac{|(S_{th}^* - \langle S_{th}^* \rangle) - (S_m^* - \langle S_m^* \rangle)|}{\sqrt{2}\sigma_m^*} \right) \quad (7)$$

$$Q = \sqrt{\frac{\sum_{i=1}^{N_s} P_i^2}{N_s}} \quad (8)$$

From Equation (4), it follows that the precision of the estimate of position and orientation strongly relates to the distance between the sensor and the tracer. Based on earlier research,<sup>30–32</sup> it is known that the maximum error for this magnetic tracer is 3 mm and for the orientation is on the order of 5–10 degrees. If the distance decreases by a factor 2, generally the error in position and orientation estimate also decreases by a factor 2. Therefore, the drum is placed close to the sensor array to maximize accuracy. With these settings, it is estimated

that the average error in position is 1 mm and in orientation 2–3 degrees.

## 2.2 | Rotating drum

The drum used in the experiments is constructed out of nonmagnetizable materials to avoid any interference with the measurements. The drum inner radius and depth are both 50 mm. The cylinder wall is made from acrylic, the two end plates are constructed from aluminum. The drum is connected to a Maxon DC motor through a Type 316 stainless steel drive shaft supported by pillow block bearings. The shaft is long enough such that the motor is placed far from the AMR sensors and does not interfere with the measurement. The motor speed is controlled by varying the voltage across its terminals and verified using a digital tachometer. A threaded hole was added to the end plate of the drum to allow the filling of the drum with (demineralized) water, which was closed with a brass bolt. The drum was overfilled and no air bubbles were found inside the drum during the experiments. Throughout the experimentation, the laboratory temperature was maintained at 20°C.

## 2.3 | Particles

The particles used in experiments were natural cork spheres. Using digital calipers, the average particle diameter was determined to be 6.3 mm (standard deviation  $\sigma = 0.14$  mm), giving a relatively small drum-to-particle size ratio of  $D/d_p \approx 16$ . This is an important factor considering continuum modeling of the system. By weighing counted samples of particles, the dry particle density was determined to be 152  $kg/m^3$ . After saturating the cork particles with water by immersing them for multiple days, a density of 295  $kg/m^3$  was measured. Before experimentation, the particles were presoaked in water, and during the measurement campaign stayed in the drum, to ensure a constant density throughout the measurements. A photograph of the cork spheres is included in Figure 1. It can be seen that the particles are not perfectly spherical and smooth, but rather show some small cracks and dents.

Table 1 shows the classification of the dry and floating beds based on the study of Courrech du Pont et al.,<sup>22</sup> placing them in the free-fall and inertial limit region, respectively. Throughout this study, the bed angle at the lowest drum speed is used as the angle of repose.<sup>33</sup>

The magnetic tracer consists of a 2.5 mm Ni-Cu-Ni-coated N42 neodymium magnet ( $\mu_m = 6.75 \times 10^{-3}$   $A \cdot m^2$ ) encapsulated in a 7.6 mm polystyrene sphere, giving it an effective density of 295  $kg/m^3$ . Despite its slightly larger diameter and density, the tracers behavior was not observed to deviate from the other particles, as was predicted by previous experimental and numerical work.<sup>34,35</sup>

## 3 | RESULTS AND DISCUSSION

In this study, experiments were conducted using beds of two different numbers of particles; 600 and 800 particles, corresponding to filling



**FIGURE 1** Cork particles used in experiments

**TABLE 1** Classification of the dry and floating bed rotating drums, based on the study of Courrech du Pont et al.<sup>22</sup>

Property	Dry	Floating	Unit
$\rho_p$	152	295	kg/m <sup>3</sup>
$\rho_f$	1.20	998	kg/m <sup>3</sup>
$\mu_f$	$1.8 \times 10^{-5}$	$1.8 \times 10^{-3}$	Pa·s
$r$	11	0.54	-
St	133	7.54	-
Regime	Free-fall	Inertial limit	

degrees of  $f = 0.35$  and  $0.45$ , respectively. Both beds were tested under dry and floating conditions using four drum speeds (20, 40, 60, and 80 RPM), leading to a total of 16 experiments. Each run was conducted for at least 1 hour, or 1200 revolutions at the lowest drum speed.

After reconstructing the tracer position and orientation from the measured magnetic field strength, the translational and rotational velocities of the single tracer were obtained by taking the respective temporal derivatives. Assuming ergodicity of the system,<sup>36</sup> the tracer position was projected onto the transverse plane of the drum and the data discretized on a grid (50 grid points across the diameter of the drum), to obtain occupancy and time-averaged translational and rotational velocities. The occupancy is defined as the probability density of finding the tracer in each cell. It is used to show that the tracer has traveled throughout the entire bed and is a good indicator of the bed shape.<sup>6,30</sup>

### 3.1 | Bed shape

Examples of the tracer occupancy, time-averaged particle velocity and average rotational velocity for the dry and floating bed drums are shown in Figures 2 and 3, respectively. These figures show measurements using 600 particles at rotational speeds of 20 and 80 RPM. A full overview of measurements including 600 and 800 particles beds and four rotational speeds is included in the Supporting Information.

Comparing the results at low and high rotational velocity in the dry bed (Figure 2), a distinct change in bed shape can be observed. At low rotation speed, the bed surface is mostly flat, while at the highest speed, a more s-shaped surface is found, tilted at a greater angle. This transformation has been observed often in previous research, for example, by Morrison et al.<sup>1</sup> The increased rate of circulation is clearly observed from the velocity profiles, revolving around a central turning point.

When making the same comparison for the floating bed (Figure 3), no change in bed shape is found. The bed surface remains mostly flat, and no change in bed angle is found. Looking at the velocity profiles, little difference between the low and high rotation speeds is found. This indicates that the bed behavior is mostly independent of the drum speed. Using 800 particles, a slight curved surface is observed at higher rotation speed.

Figures 2 and 3C,F show the particle angular velocity  $\omega$  in the transverse plane of the drum, normalized by the drum rotation rate  $\Omega$ . Positive values indicate a clockwise rotation, along with the drum. At lower drum speed, tumbling of the particles occurs only at the bed surface, while the particles close to the wall undergo solid-body rotation with the drum ( $\omega/\Omega = 1$ ). At higher drum speeds, tumbling of the particles is less pronounced, as particles get projected into the drum rather than rolling of the bed surface. In the floating bed drum, a band of higher angular velocity is observed close to the drum, whereas particles further into the bed exhibit under-rotation ( $\omega/\Omega \approx 0.5$ ). This remarkable feature shows how the reduced friction due to the presence of water allows for relative particle motion, even in densely packed regions.

A distinct band of low occupancy close to the wall in the lower half of the bed is found in nearly all floating bed measurements, and to a lesser degree in the dry bed. The band is located at approximately  $1 d_p$  distance from the drum wall. This suggests a structured stacking of particles against the wall, or wall exclusion effect. Unfortunately, further investigation of this phenomenon using particle tracking methods is precarious, as no information on the particles surrounding the tracer is available. Tomographic or numerical methods are better suited for such an investigation.

The definitions used for further analysis of the bed behavior are shown schematically in Figure 4. Here,  $O$  indicates the drum center and  $\alpha$  the bed angle, which is determined at the midpoint along the surface of the bed. The surface point  $S$  is defined as the position along  $OC$  beyond which 99% of measurements are located. This also fixes the line along the bed surface  $AB$ . Finally, turning point  $T$  is defined as the point along  $OC$  where its crosswise velocity changes direction.

The observed bed angles measured in dry and floating bed drums are plotted in Figure 5. An increase of bed angle with increasing rotation rate is observed for the dry bed, which levels off at the highest drum speed. This increase was previously observed in both experiments and numerical simulations.<sup>4,37</sup> The floating bed shows a different behavior entirely. For the 600 particle floating bed, no increase of bed angle is observed. The floating bed of 800 particles exhibits an initial increase in bed angle, but no further increase at higher drum speeds. These findings correspond with the observed bed slippage, which is discussed in Section 3.2.

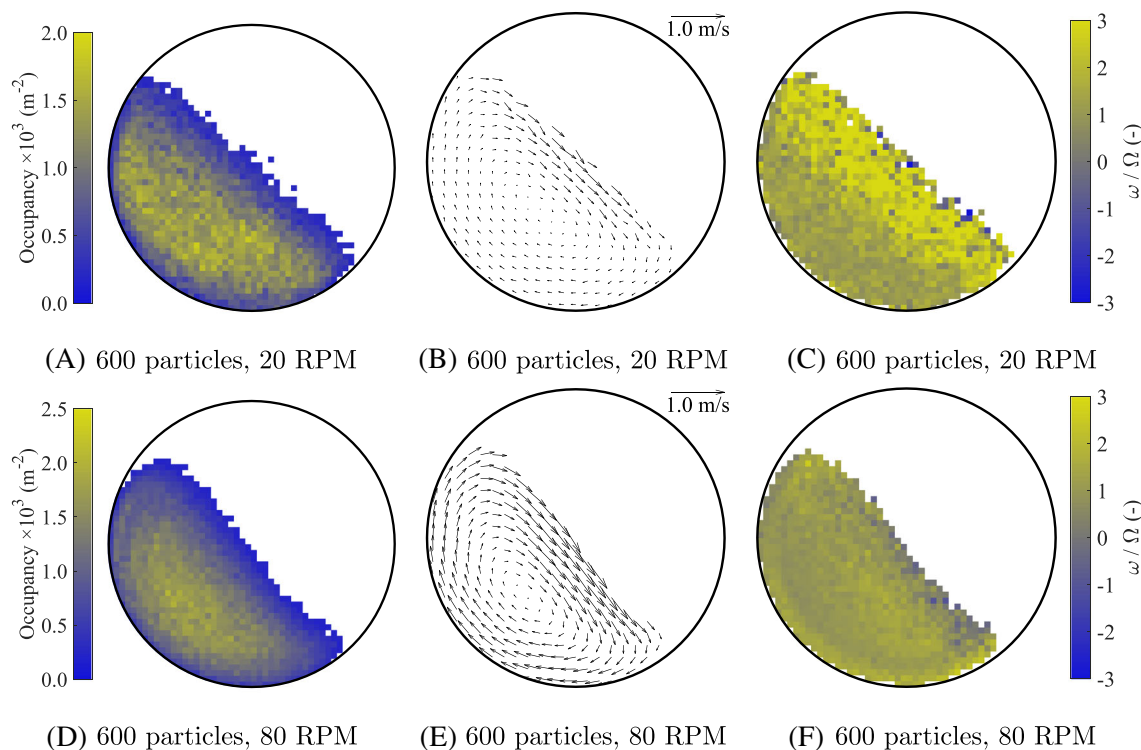


**FIGURE 2** Time-average bed occupancy, particle velocity profiles, and particle angular velocity for the dry rotating drum containing 600 particles, at 20 RPM (A-C) and 80 RPM (D-F)

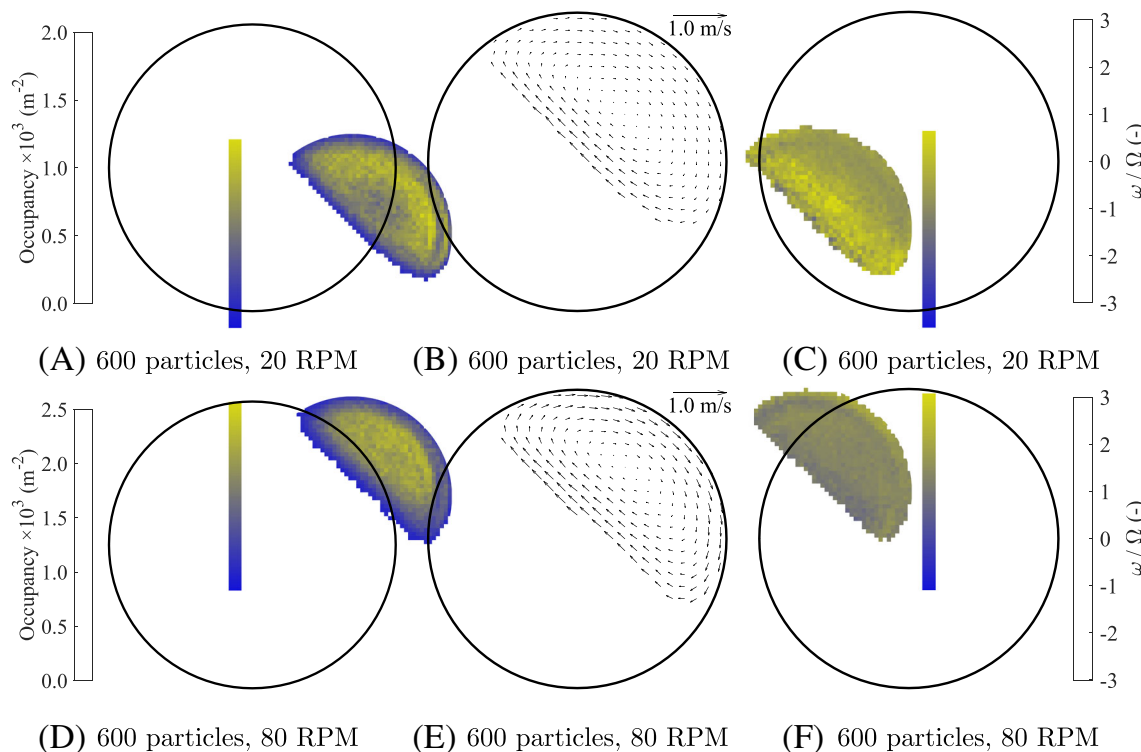


**FIGURE 3** Time-average bed occupancy, particle velocity profiles, and particle angular velocity for the floating bed rotating drum containing 600 particles, at 20 RPM (A-C) and 80 RPM (D-F)

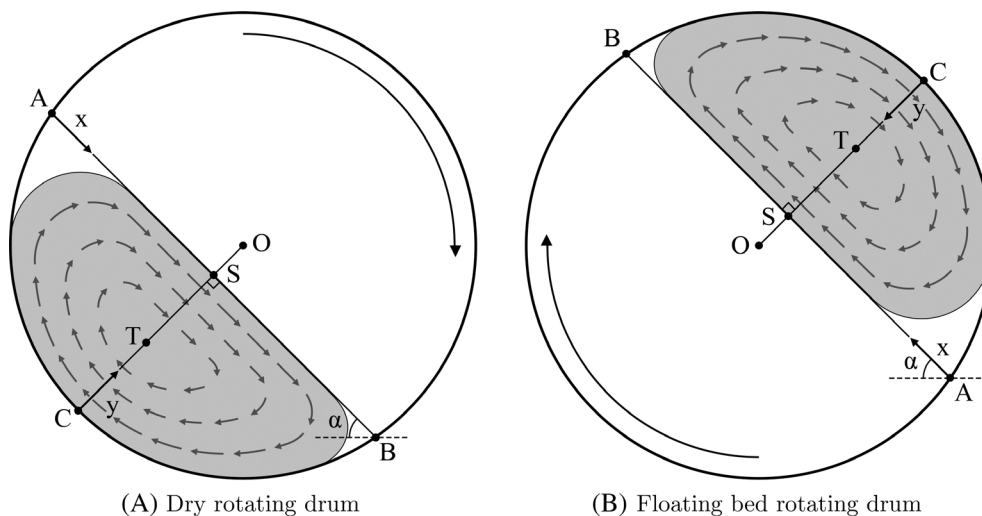


**FIGURE 4** Schematic overview of the rotating drum, indicating bed angle  $\alpha$ , drum center O, bed surface AB, turning point T, and bed depth CS. The coordinate system used in this study is indicated

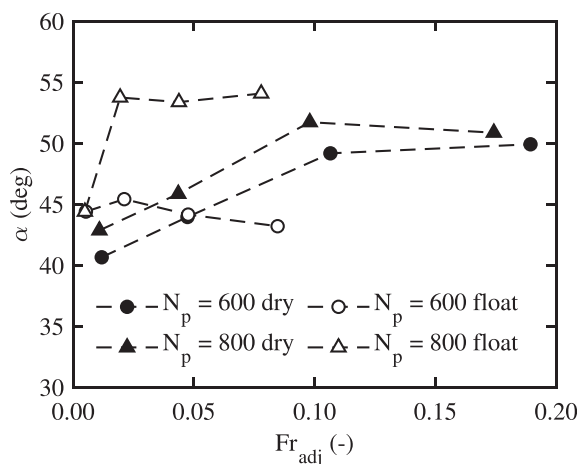


**FIGURE 5** Observed bed angle plotted against adjusted Froude number (Equation 3) for dry and floating bed rotating drums

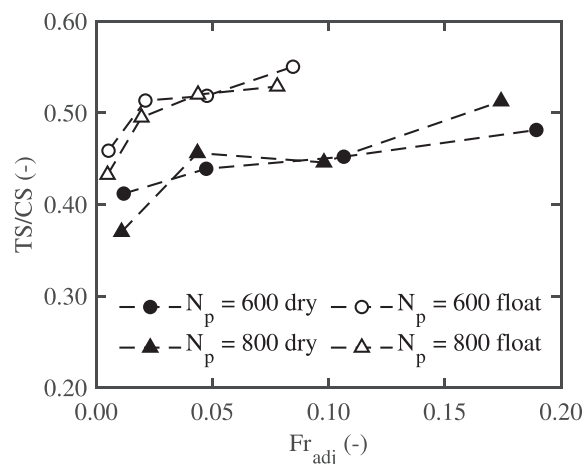


**FIGURE 7** Observed active layer depth relative to total bed depth, plotted against adjusted Froude number (Equation 3) for dry and floating bed rotating drums

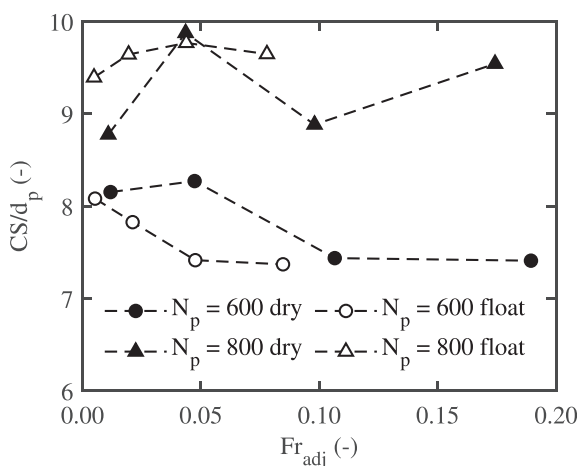


**FIGURE 6** Observed total bed depth normalized by  $d_p$ , plotted against adjusted Froude number (Equation 3) for dry and floating bed rotating drums

The total bed depth (CS, Figure 4) can be divided in a passive layer close to the drum wall (CT) and an active layer closer to the bed surface (TS). Figure 6 shows the total bed depth CS expressed in  $d_p$  for both the dry and floating bed drums, whereas Figure 7 shows the active layer depth relative to the total bed depth. While the layer depth measurement is highly sensitive to method chosen for determination of the surface point S, general trends are clearly visible.

The total bed depth CS is found to decrease slightly with drum speed for the lower filling degree, and increase for the higher filling degree. The trend is not captured well by the adjusted Froude number, indicating that physics other than gravity govern this effect. The exact underlying mechanics are not evident from this study, as more microscopic information on the particle–particle contact would be required to uncover this.

For the active layer depth, the lines for both bed sizes collapse reasonable well. However, the floating bed shows a significantly larger

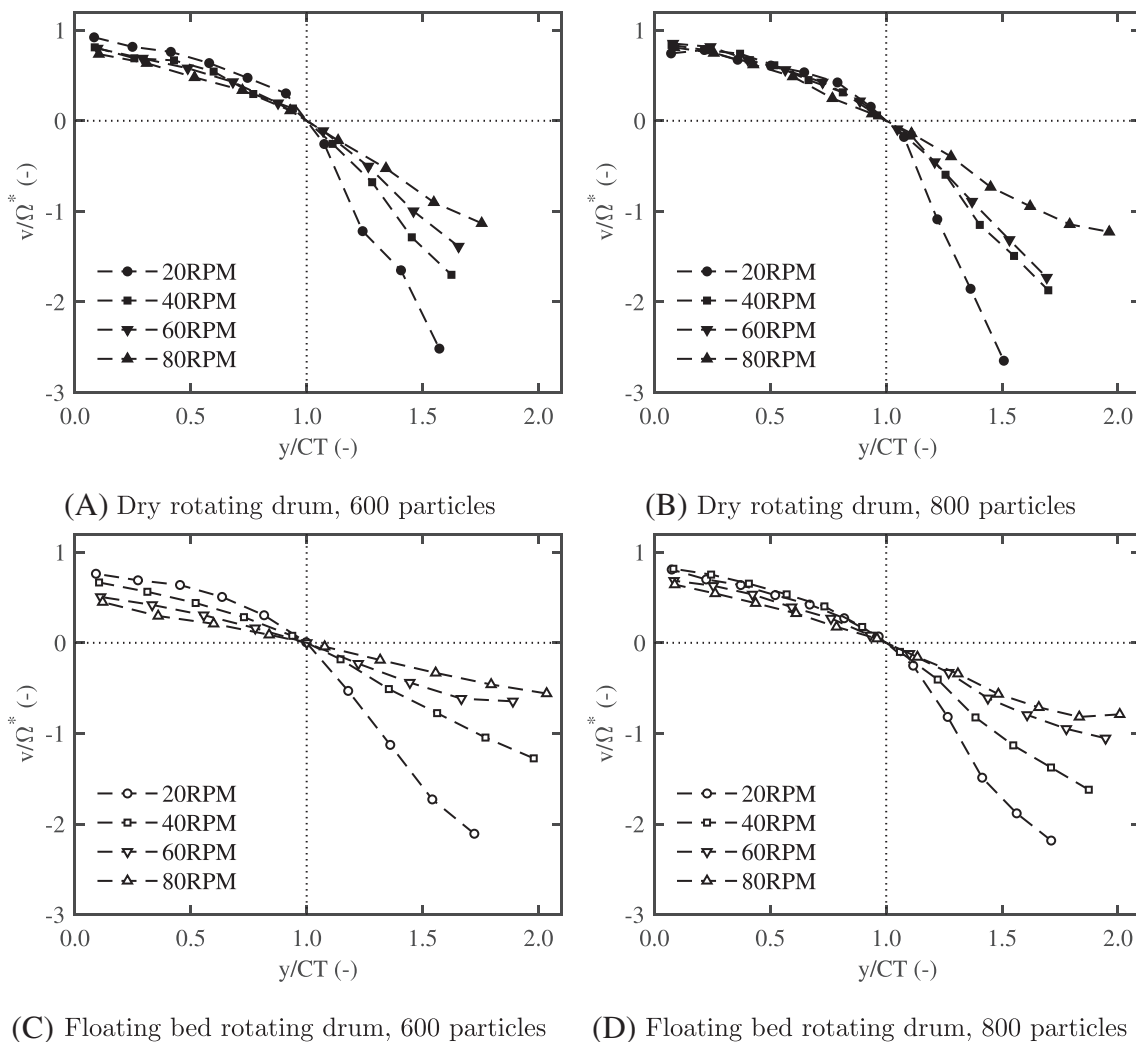


**FIGURE 8** Particle velocity profile (perpendicular to CS, Figure 4) plotted over the bed depth for dry and floating bed rotating drums, 600 and 800 particles. The wall point C corresponds with  $y/CT = 0$

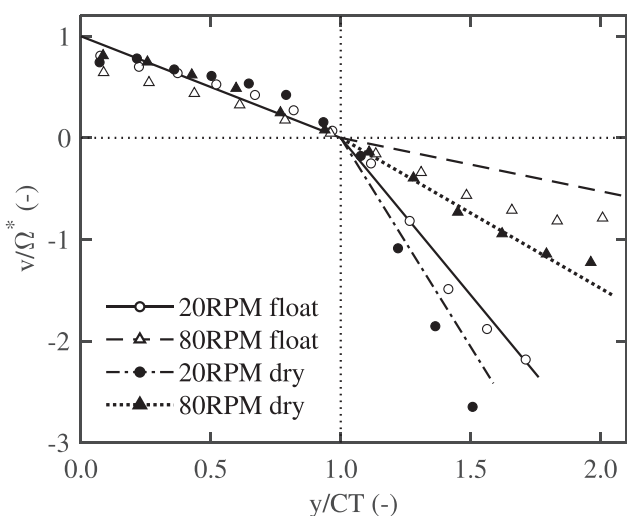


**FIGURE 9** Comparison of dry and floating particle velocity profiles perpendicular to CS (Figure 4) using 800 particles and two different drum speeds. Lines indicate bilinear profiles with maximum surface velocities given by Equations (9) and (10). The wall point C corresponds with  $y/CT = 0$

active layer depth than the dry bed. Boateng and Barr<sup>38</sup> observed an expansion of the active layer with increasing drum speed. Such an increase is observed for dry and floating beds, both in absolute layer depth and relative to the total bed depth. The floating bed shows a steeper initial increase before leveling off, whereas the dry bed shows steady expansion over the whole range of measured Froude numbers. It must be noted however that some reservation must be made with the analysis on the bed depths since the bed is generally just 7–10 particle diameters thick. The general trend however seems to agree with what is found in literature for larger drums.<sup>38</sup>

### 3.2 | Particle velocities

The time-averaged particle velocity is a property of great interest in rotating drum research. Two commonly report velocity profiles are the crosswise velocity along the bed depth, defined as the component perpendicular to CS (Figure 4) and the streamwise velocity along the



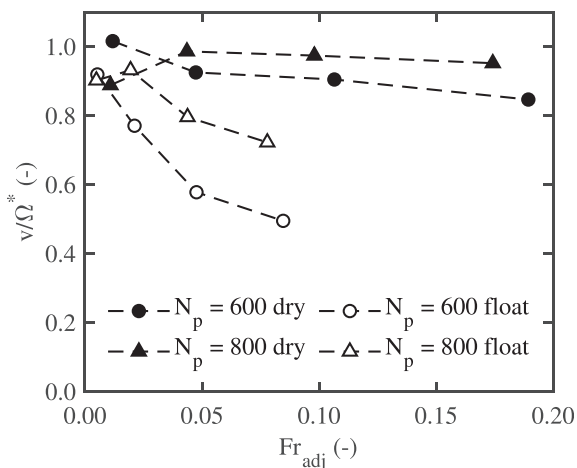


**FIGURE 10** Particle velocity extrapolated to the wall position, normalized by the drum wall velocity and plotted against adjusted Froude number for dry and floating bed rotating drums

bed surface, parallel to AB. These two profiles are shown in Figures 8 and 11, respectively.

The velocity profile along the bed depth is commonly assumed to be comprised of two linear sections separated by the turning point.<sup>2</sup> Similar profile shapes can be observed in Figure 8, for both the dry and floating beds. The linear section in the passive layer corresponds with a solid body rotation along with the drum wall, whereas the profile in the active layer linearly approaches the maximum surface velocity  $v_s$ .

Khakhar et al.<sup>39</sup> derived the model for the maximum surface velocity in the dry case given by Equation (9), where AB and TS (Figure 4) are the surface length and active layer depth, respectively. For immersed particles in the inertial limit regime, Courrech Du Pont et al.<sup>22</sup> defined the terminal particle velocity based on the balance of drag, gravity and buoyancy forces, Equation (10). Per illustration, Figure 9 shows a comparison between dry and floating particle velocity profiles, using 800 particles and drum speeds of 20 and 80 RPM. Here, the lines indicate bilinear velocity profiles with maximum

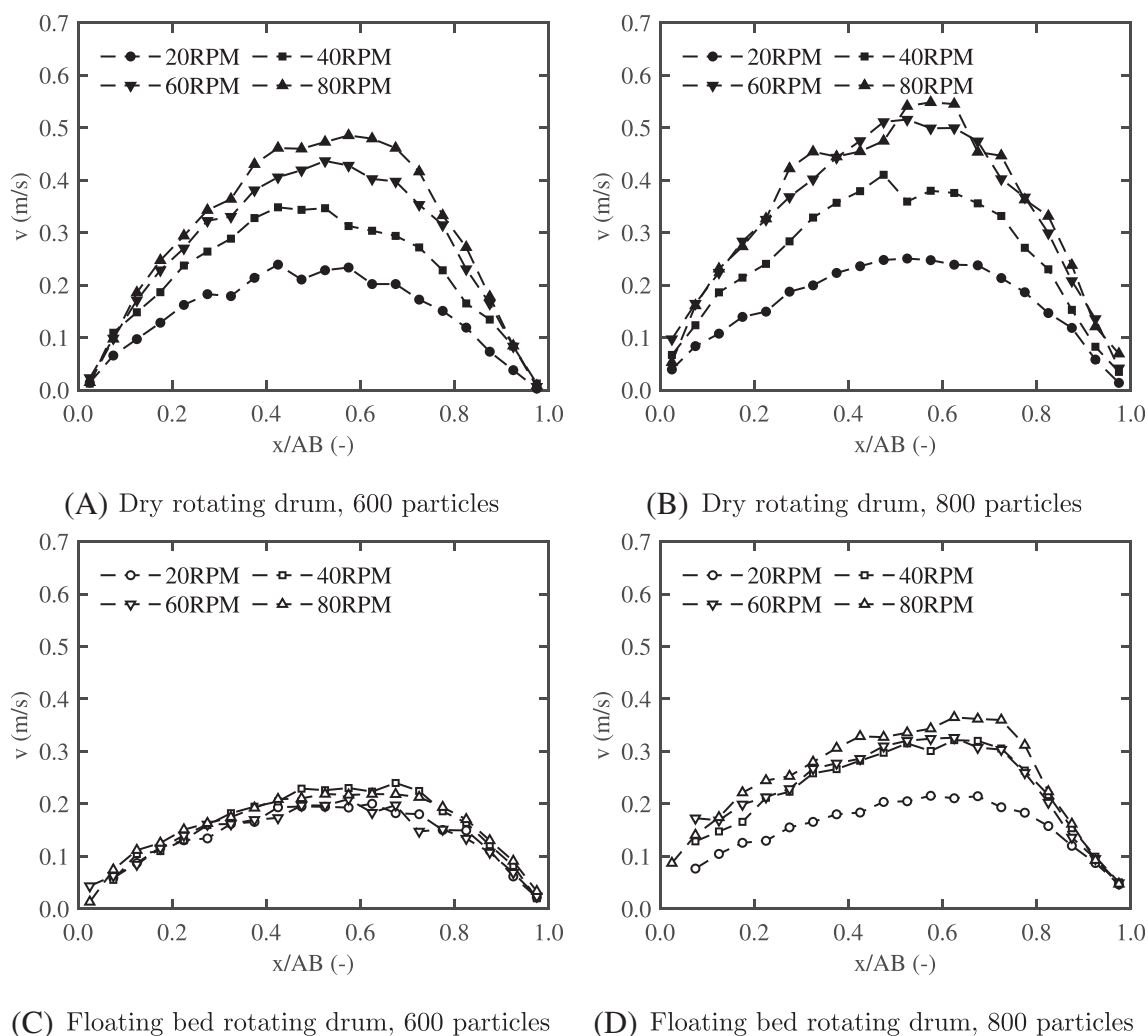


**FIGURE 11** Particle velocity profile plotted over the bed surface (parallel to AB, Figure 4) for dry and floating bed rotating drums, 600 and 800 particles. The points A and B correspond with  $x/AB = 0$  and  $x/AB = 1$ , respectively

surface velocities given by Equations (9) and (10) for the dry and floating cases, respectively.

$$v_{s,dry} = \frac{\Omega(AB/2)^2}{TS} \quad (9)$$

$$v_{s,inertial} = \sqrt{\frac{2\Delta\rho g d_p \sin\theta}{\rho_f}} \quad (10)$$

From Figure 9, the measured dry bed velocity profiles can be seen to correspond reasonably well with the profile predicted by Equation (9). Likewise, the floating bed velocity profile is predicted very well by Equation (10) at low drum speed. However, at high drum speed the measured velocities deviate significantly from the predicted line, both in shape and magnitude. Clearly, particles move faster than their terminal velocity given by Equation (10). This indicates that the model of single particles moving through a stagnant liquid is not appropriate, and a macroscopic movement of liquid along the flowing particle layer occurs. The flattening of the velocity profile at the surface suggests particles near the bed surface experience a stronger interaction with the liquid than particles deeper into the bed. As the current method does not provide insight into the liquid behavior, we highly recommend further research into this interaction. Especially numerical methods<sup>40</sup> are suitable for gaining insight in the complex interaction between the solid and liquid phases.

Another striking difference between the dry and floating bed is found when comparing the particle velocity close to the wall with the linear wall velocity  $\Omega^* = \Omega R$ . This is detailed in Figure (10), in which the particle velocity profile is linearly extrapolated to the wall position and compared with the drum wall velocity. In the dry case, a small degree of slip between the particles and the wall is observed. This is most pronounced at the lower particle count and higher drum velocity, stemming from the decreased friction of the lighter bed. For the floating bed, a much higher degree of slip is observed, up to a 50% velocity difference. Again, this is most pronounced at high velocity and low particle count, as the larger bed exerts a larger buoyancy on the wall. This large difference between the dry and floating cases indicates that the presence of liquid significantly alters the interaction between particles and the drum wall.

The particle velocity profile along the bed surface in a dry rotating drum is commonly described as a parabolic shape, which tends to skew toward the bottom of the bed at higher drum speed.<sup>38</sup> The same observations can be made from Figure 11. In these plots,  $-1$  and  $1$  on the horizontal axis correspond to  $A$  and  $B$ , respectively (Figure 4), following the path of the particles. For the dry bed, the parabolic profile increases in magnitude with increasing drum speed, and skews slightly to the right at the highest rotation speeds. Furthermore, little difference is found between the profiles for both filling degrees.

The surface velocity profile for the floating bed is also of parabolic shape, displaying slightly more skewness than the dry bed. However, its magnitude does not increase steadily with increasing drum speed. Instead, hardly any increase is found for the 600 particle bed. The 800 particle bed only displays an increase in surface velocity

between 20 and 40 RPM. This same trend was observed for the bed angle shown in Figure 5. As discovered previously from Figure 10, the floating bed exhibits a large degree of slip with respect to the drum wall. Therefore, no additional kinetic energy is transferred to the particle bed, leading to little increase in particle velocity with increased drum speed.

## 4 | CONCLUSIONS AND OUTLOOK

A study on the behavior of floating particle beds in a rotating drum was conducted using MPT. Experiments using both dry and floating cork particles were performed, spanning two filling degrees and two rotational speeds. The modified Froude number of the two systems are of the same order, indicating that gravitational effects relative to the rotation of the drum operate in similar regimes. Alternatively by assessment of the Stokes number it was shown that the dry granular bed was operating in the free fall regime, while the floating bed was operated in an inertial regime, which proves that for the liquid case the interstitial fluid, physically, cannot be ignored.

Occupancy, particle velocity, and angular velocity plots were obtained, showing the bed shape and circulation in each experiment. For the dry bed, particle rotation was found to follow a solid body rotation along the drum wall. In the floating case, a difference in particle angular velocity was found between particles close to the drum wall and deeper into the passive layer. This relative motion of particles was attributed to the decreased particle–particle friction stemming from the presence of water.

The bed angle was shown to increase with rotation speed for the dry bed, leveling off at the highest rotational speed. For the floating case, no increase in bed angle was found at low filling degree, and only an initial increase at the higher filling degree. This shows how decreased friction renders the bed behavior largely insensitive to increased drum speeds. Furthermore, it was shown that liquid presence gives rise to a more expanded state of the active layer. These findings indicate that the presence of water significantly alters the particle–wall and particle–particle interactions, and thereby influence the macroscopic bed behavior. This influence is not well captured by current models, such as the adjusted Froude number<sup>24</sup> employed in this study.

The velocity profiles along the bed depth obtained for the dry and floating beds were of similar shape, showing largely linear profiles in the active and passive layer. However, at high drum speeds particles close to the wall were found not to follow the drum rotation, slipping with respect to the wall instead. This degree of slippage was investigated and found to be more pronounced in the floating case. A lower degree of slip was found at the higher filling degree due to the increased buoyancy. Due to this slip behavior, little increase in particle velocity was observed with increasing bed velocity.

The maximum particle velocity at the bed surface was compared with existing models for the dry<sup>39</sup> and inertial-limited<sup>22</sup> floating cases. Results for the dry bed were found to match reasonably well. The floating bed, however, exhibited particle velocities significantly larger

than the predicted terminal velocity at high drum speed. Clearly, the model of single particles moving through a stationary liquid<sup>22</sup> is not applicable, and a macroscopic liquid flow occurs along the bed surface. Furthermore, the particle velocity close to the bed surface was found to deviate from the linear shape, indicating a strong liquid-particle interaction is felt at the surface than deeper into the bed.

Analysis of the velocity profile along the bed surface shows mostly parabolic profiles for both the dry and floating beds. The profiles skew toward the end of the surface at higher velocity, and do so more in the case of the floating bed. Again, a diminishing increase of particle velocity with higher drum velocity was observed for the floating case, confirming observations made from the bed angle.

In conclusion, the effect of the interstitial medium on rotating drum behavior, as its density surpasses that of the particles, is a complex phenomenon which cannot be captured by considering an effective gravity. The altered particle-particle and particle-wall interactions are of paramount importance for particle behavior, both in the passive and active layers. Coincidentally, the viscous and inertial liquid-solid interactions play a key role within the flowing layer, which remains largely ill-understood.

For the further study of floating bed rotating drums and liquid-solid systems in general, the authors recommend exploration of different relative densities of the particles and liquid. By means of study of the balance between particle and liquid inertia, as well as liquid viscosity, much can be learned about the interaction of particles and their surrounding medium. In this study, the slippage between the drum wall and particles has been shown of great importance to the bed behavior. The particle shape and surface roughness are expected to play a key role in this, and will prove interesting subjects of study. This also includes the study of side wall effects, which likely play a role at the current system size.

Finally, the detailed measurements provided by MPT in this study are well suited for comparison with numerical simulations. The dynamic particle behavior in the rotating drum environment is an excellent validation case for multiphase flow models, such as the various frameworks presented in recent literature.<sup>40-44</sup>

## ACKNOWLEDGMENTS

The authors thank Tata Steel Europe for their financial support for this project. This research was carried out under project number S16046 in the framework of the Partnership Program of the Materials innovation institute M2i ([www.m2i.nl](http://www.m2i.nl)) and the Technology Foundation STW ([www.stw.nl](http://www.stw.nl)), which is part of the Netherlands Organization for Scientific Research ([www.nwo.nl](http://www.nwo.nl)).

## CONFLICT OF INTEREST

The author declares that there is no conflict of interest that could be perceived as prejudicing the impartiality of the research reported.

## AUTHOR CONTRIBUTIONS

**Tim M.J. Nijssen:** Conceptualization (equal); data curation (equal); formal analysis (equal); investigation (equal); methodology (equal); validation (equal); visualization (equal); writing – original draft (equal). **Mark a.h. van Dijk:** Data curation (equal); formal analysis (equal); investigation (equal). **J.A.M. (Hans) Kuipers:** Funding acquisition (equal); supervision (equal);

writing – review and editing (equal). **Jan van der Stel:** Funding acquisition (equal); supervision (equal); writing – review and editing (equal). **Allert T. Adema:** Funding acquisition (equal); supervision (equal); writing – review and editing (equal). **Kay A Buist:** Conceptualization (equal); funding acquisition (equal); methodology (equal); project administration (equal); supervision (equal); writing – review and editing (equal).

## DATA AVAILABILITY STATEMENT

The data that support the findings of this study are openly available in 4TU.ResearchData at <http://doi.org/10.4121/13721104>.

## ORCID

Tim M. J. Nijssen  <https://orcid.org/0000-0002-2574-8547>

Kay A. Buist  <https://orcid.org/0000-0003-1765-576X>

## REFERENCES

- Morrison A, Govender I, Mainza A, Parker D. The shape and behaviour of a granular bed in a rotating drum using Eulerian flow fields obtained from PEPT. *Chem Eng Sci.* 2016;152:186-198.
- Alizadeh E, Dubé O, Bertrand F, Chaouki J. Characterization of mixing and size segregation in a rotating drum by a particle tracking method. *AIChE J.* 2013;59:1894-1905.
- Norouzi HR, Zarghami R, Mostoufi N. Insights into the granular flow in rotating drums. *Chem Eng Res Des.* 2015;102:12-25.
- Yang RY, Zou RP, Yu AB. Microdynamic analysis of particle flow in a horizontal rotating drum. *Powder Technol.* 2003;130:138-146.
- Oschmann T, Kruggel-Emden H. A novel method for the calculation of particle heat conduction and resolved 3D wall heat transfer for the CFD/DEM approach. *Powder Technol.* 2018;338:289-303.
- Dubé O, Alizadeh E, Chaouki J, Bertrand F. Dynamics of non-spherical particles in a rotating drum. *Chem Eng Sci.* 2013;101:486-502.
- Brewster R, Grest GS, Levine AJ. Effects of cohesion on the surface angle and velocity profiles of granular material in a rotating drum. *Phys Rev E Stat Nonlinear Soft Matter Phys.* 2009;79:1-7.
- Ding YL, Forster RN, Seville JP, Parker DJ. Some aspects of heat transfer in rolling mode rotating drums operated at low to medium temperatures. *Powder Technol.* 2001;121:168-181.
- Schutyser MA, Weber FJ, Briels WJ, Rinzema A, Boom RM. Heat and water transfer in a rotating drum containing solid substrate particles. *Biotechnol Bioeng.* 2003;82:552-563.
- Shibasaki N, Hirose K, Yonemoto T, Tadaki T. Suspension culture of *Nicotiana tabacum* cells in a rotary-drum bioreactor. *J Chem Technol Biotechnol.* 1992;53:359-363.
- Banerjee DK, Fedorak PM, Hashimoto A, Masliyah JH, Pickard MA, Gray MR. Monitoring the biological treatment of anthracene-contaminated soil in a rotating-drum bioreactor. *Appl Microbiol Biotechnol.* 1995;43:521-528.
- Herrera MN, Escobar B, Parra N, González C, Vargas T. Bioleaching of refractory gold concentrates at high pulp densities in a nonconventional rotating-drum reactor. *Miner Metall Process.* 1998;15:15-19.
- Jin J, Liu GL, Shi SY, Cong W. Studies on the performance of a rotating drum bioreactor for bioleaching processes – oxygen transfer, solids distribution and power consumption. *Hydrometallurgy.* 2010;103:30-34.
- Loi G, Rossi A, Trois P, Rossi G. Continuous revolving barrel bioreactor tailored to the bioleaching microorganisms. *Miner Metall Process.* 2006;23:196-202.
- Cabrera MA, Gollin D, Kaitna R, Wu W. Viscous effects on granular mixtures in a rotating drum. In: Wu W, ed. *Recent Advances in Modeling Landslides and Debris Flows.* Springer International Publishing; 2015:57, 71.

16. Schneider D, Kaitna R, Dietrich WE, Hsu L, Huggel C, McArdell BW. Frictional behavior of granular gravel–ice mixtures in vertically rotating drum experiments and implications for rock–ice avalanches. *Cold Reg Sci Technol*. 2011;69:70-90.
17. Caballero L, Sarocchi D, Borselli L, Cárdenas AI. Particle interaction inside debris flows: evidence through experimental data and quantitative clast shape analysis. *J Volcanol Geotherm Res*. 2012;231–232: 12-23.
18. Breu AP, Kruelle CA, Rehberg I. Pattern formation in a rotating aqueous suspension. *Europhys Lett*. 2003;62:491-497.
19. Breu AP, Kruelle CA, Rehberg I. Oscillatory patterns in a rotating aqueous suspension. *Eur Phys J E*. 2004;13:189-196.
20. Jain N, Khakhar DV, Lueptow RM, Ottino JM. Self-organization in granular slurries. *Phys Rev Lett*. 2001;86:3771-3774.
21. Finger T, Stannarius R. Influences of the interstitial liquid on segregation patterns of granular slurries in a rotating drum. *Phys Rev E Stat Nonlinear Soft Matter Phys*. 2007;75:1-9.
22. Courrech du Pont S, Gondret P, Perrin B, Rabaud M. Granular avalanches in fluids. *Phys Rev Lett*. 2003;90(4):044301.
23. Jain N, Ottino JM, Lueptow RM. Effect of interstitial fluid on a granular flowing layer. *J Fluid Mech*. 2004;508:23-44.
24. Juarez G, Chen P, Lueptow RM. Transition to centrifuging granular flow in rotating tumblers: a modified Froude number. *New J Phys*. 2011;13(5):053055.
25. Liao CC, Hsiao SS, To K. Granular dynamics of a slurry in a rotating drum. *Phys Rev E Stat Nonlinear Soft Matter Phys*. 2010;82:2-5.
26. Liao CC, Lan HW, Hsiao SS. Density-induced granular segregation in a slurry rotating drum. *Int J Multiphase Flow*. 2016;84:1-8.
27. Chou SH, Liao CC, Hsiao SS. The effect of interstitial fluid viscosity on particle segregation in a slurry rotating drum. *Phys Fluids*. 2011;23: 083301.
28. Chou SH, Hsiao SS. Dynamic properties of immersed granular matter in different flow regimes in a rotating drum. *Powder Technol*. 2012; 226:99-106.
29. Parsons TG, Masliyah JH, Gray MR. Solid-liquid mass transfer in a rotary drum. *Can J Chem Eng*. 2001;79:726-731.
30. Buist KA, Gaag AC, Deen NG, Kuipers JAM. Improved magnetic particle tracking technique in dense gas fluidized beds. *AIChE J*. 2014;60: 3133-3142.
31. Buist KA, Erdewijk TW, Deen NG, Kuipers JAM. Determination and comparison of rotational velocity in a pseudo 2-D fluidized bed using magnetic particle tracking and discrete particle modeling. *AIChE J*. 2015;61:3198-3207.
32. Yang L, Padding J, Buist K, Kuipers J. Three-dimensional fluidized beds with rough spheres: validation of a two fluid model by magnetic particle tracking and discrete particle simulations. *Chem Eng Sci*. 2017;174:238-258.
33. Carrigy MA. Experiments on the angles of repose of granular materials. *Sedimentology*. 1970;14:147-158.
34. Jain N, Ottino JM, Lueptow RM. Regimes of segregation and mixing in combined size and density granular systems: an experimental study. *Granul Matter*. 2005;7:69-81.
35. Yari B, Beaulieu C, Sauriol P, Bertrand F, Chaouki J. Size segregation of bidisperse granular mixtures in rotating drum. *Powder Technol*. 2020;374:172-184.
36. Wildman RD, Huntley JM, Hansen JP, Parker DJ, Allen DA. Single-particle motion in three-dimensional vibrofluidized granular beds. *Phys Rev E Stat Phys Plasmas Fluids Relat Interdiscip Topics*. 2000;62:3826-3835.
37. Yamane K, Nakagawa M, Altobelli SA, Tanaka T, Tsuji Y. Steady particulate flows in a horizontal rotating cylinder. *Phys Fluids*. 1998;10: 1419-1427.
38. Boateng AA, Barr PV. Granular flow behaviour in the transverse plane of a partially filled rotating cylinder. *J Fluid Mech*. 1997;330:233-249.
39. Khakhar DV, McCarthy JJ, Ottino JM. Radial segregation of granular mixtures in rotating cylinders. *Phys Fluids*. 1997;9:3600-3614.
40. Maitri RV, Das S, Kuipers JA, Padding JT, Peters EA. An improved ghost-cell sharp interface immersed boundary method with direct forcing for particle laden flows. *Comput Fluids*. 2018;175:111-128.
41. Barker T, Rauter M, Maguire ES, Johnson CG, Gray JM. Coupling rheology and segregation in granular flows. *J Fluid Mech*. 2021;909:A22-1-A22-46.
42. Yang LY, Zheng QJ, Yu AB. Numerical simulation of solid flow and segregation in a blast furnace by coupling granular rheology and transport equation. *Chem Eng Sci*. 2021;242:116741.
43. Liu Y, Gonzalez M, Wassgren C. Modeling granular material segregation using a combined finite element method and advection-diffusion-segregation equation model. *Powder Technol*. 2019;346:38-48.
44. Rauter M. The compressible granular collapse in a fluid as a continuum: validity of a Navier-stokes model with,  $\mu(J)$ ,  $\phi(J)$ -rheology. *J Fluid Mech*. 2021;915:1-42.

#### SUPPORTING INFORMATION

Additional supporting information may be found in the online version of the article at the publisher's website.

**How to cite this article:** Nijssen TMJ, van Dijk MAH, Kuipers HAM, van der Stel J, Adema AT, Buist KA. Experiments on floating bed rotating drums using magnetic particle tracking. *AIChE J*. 2022;68(5):e17627. doi:10.1002/aic.17627